Abnormal sterols in cholesterol-deficiency diseases cause secretory granule malformation and decreased membrane curvature

Marjorie C. Gondré-Lewis[1,*], Horia I. Petrache[2], Christopher A. Wassif[3], Daniel Harries[2], Adrian Parsegian[2], Forbes D. Porter[3] and Y. Peng Loh[1,‡]

[1]Section on Cellular Neurobiology, [2]Laboratory of Physical and Structural Biology and [3]Heritable Disorders Branch, National Institute of Child Health and Human Development, NIH, Bethesda, MD 20892, USA

*Present address: Department of Anatomy, Howard University College of Medicine, Washington, DC 20059, USA
‡Author for correspondence (e-mail: lohp@mail.nih.gov)

Accepted 27 January 2006
Journal of Cell Science 119, 1876-1885 Published by The Company of Biologists 2006
doi:10.1242/jcs.02906

Summary

Cholesterol is an abundant lipid in eukaryotic membranes, implicated in numerous structural and functional capacities. Here, we have investigated the mechanism by which cholesterol affects secretory granule biogenesis in vivo using *Dhcr7*$^{-/-}$ and *Sc5d*$^{-/-}$ mouse models of the human diseases, Smith-Lemli-Opitz syndrome (SLOS) and lathosterolosis. These homozygous-recessive multiple-malformation disorders are characterized by the functional absence of one of the last two enzymes in the cholesterol biosynthetic pathway, resulting in the accumulation of precursors. Cholesterol-deficient mice exhibit a significant decrease in the numbers of secretory granules in the pancreas, pituitary and adrenal glands. Moreover, there was an increase in morphologically aberrant granules in the exocrine pancreas of *Dhcr7*$^{-/-}$ acinar cells. Regulated secretory pathway function was also severely diminished in these cells, but could be restored with exogenous cholesterol. Sterol precursors incorporated in artificial membranes resulted in decreased bending rigidity and intrinsic curvature compared with cholesterol, thus providing a cholesterol-mediated mechanism for normal granule budding, and an explanation for granule malformation in SLOS and lathosterolosis.

Key words: Cholesterol, Granule biogenesis, Membrane curvature, Regulated secretory pathway, Smith-Lemli-Opitz syndrome (SLOS), Lathosterolosis

Introduction

Cholesterol is a crucial player at the subcellular level in defining functional membrane microdomains for cellular activity (Schrader, 2004; van Meer, 1993). Studies in endocrine and other cells have suggested that cholesterol may be necessary for vesicle biogenesis at the trans-Golgi network (TGN), which contains cholesterol-sphingolipid-rich microdomains from which dense core granules (DCGs) bud (Keller and Simons, 1998; Loh et al., 2004; Tooze, 1998; Wang et al., 2000). In neurons, endocrine and exocrine cells, secreted proteins include processed neuropeptides, hormones and enzymes which are packaged into DCGs and released upon stimulation via the regulated secretory pathway (RSP) (Thiele and Huttner, 1998). Thus DCG formation is essential for higher-order physiological function.

Inborn errors of cholesterol synthesis lead to developmental abnormalities, including mental retardation, and the most common of these genetic diseases is Smith-Lemli-Opitz Syndrome (SLOS). SLOS is an autosomal-recessive, multiple malformation and/or mental retardation syndrome in which the function of the enzyme, 7-dehydrocholesterol reductase (DHCR7), necessary for the final step of cholesterol biosynthesis, is impaired (Porter, 2000; Tint et al., 1994). SLOS reportedly affects 1:10,000 to 1:40,000 caucasian Americans and is caused by mutations in the gene encoding *DHCR7* with the severity of disease dependent on the type of mutation (Witsch-Baumgartner et al., 2001). Another inborn error of cholesterol synthesis is lathosterolosis. Patients with lathosterolosis lack lathosterol-5-desaturase (SC5D), the enzyme that catalyzes the next-to-last step in cholesterol synthesis. Lathosterolosis is a rare disorder and to date has only been identified in two patients (Brunetti-Pierri et al., 2002; Krakowiak et al., 2003). Currently little is known about the pathology of these diseases in humans. Mouse models of SLOS and lathosterolosis were developed in our laboratory to investigate the importance of cholesterol in cellular function in vivo and to study the pathology of the equivalent human syndromes.

Given the importance of cholesterol as a major component of lipid rafts, and the dependence on lipid raft microdomains for DCG formation, we investigated secretory granule biogenesis in vivo using SLOS and lathosterolosis mouse models. The aim of this study was threefold: first, to determine how sterol content of membranes impacts DCG biogenesis and regulated secretion; second, to examine how, mechanistically, cholesterol, 7-dehydrocholesterol (7-DHC) and lathosterol affect membrane curvature and granule formation; third, to understand the pathophysiology of cholesterol-defective diseases.

In this work, we present evidence demonstrating that

Journal of Cell Science

Journal of Cell Science

impairment of the cholesterol biosynthetic pathway results in absent or aberrant granule formation, and impairment of secretion in vivo in exocrine pancreas. We further show that formation of endocrine granules in the pituitary and adrenals are also compromised. Substitution of other sterols, i.e. 7-DHC and lathosterol, for cholesterol in *Dhcr7*$^{-/-}$ and *Sc5d*$^{-/-}$ mice, respectively, was not sufficient to rescue the RSP and caused abnormal membrane characteristics attributed to the reduced rigidity of these sterols as determined by small-angle X-ray scattering methods. These findings clearly demonstrate that cholesterol is essential for conferring the rigidity necessary for membrane curvature during secretory granule biogenesis in vivo.

Results

Sterol structures and content in cholesterol-deficient mouse models.

The cholesterol biosynthetic disorders, SLOS and lathosterolosis, are respectively caused by defective enzymatic function of DHCR7 and SC5D in the final two steps in the Kandutsch-Russell cholesterol synthetic pathway (Fig. 1A). Examination of the chemical structure for cholesterol, 7-DHC and lathosterol reveals differences between cholesterol and lathosterol only in the location of the double bond, and between cholesterol and 7-DHC, in the number of double bonds in the sterol ring, possibly altering contribution to membrane structure (note that the positions of the bonds affects the planar structure found in cholesterol). In each case, the sterol immediately upstream of the inactive enzyme is accumulated in tissues. Cholesterol is an abundant lipid and accounts for nearly 100% of sterols in all tissues, including the pancreas of normal animals (Fig. 1B), whereas levels of lathosterol, 7-DHC and 8-DHC are negligible at steady state (Fig. 1B). Pancreatic tissue from *Dhcr7*$^{-/-}$ mice showed dramatically increased levels of 7-DHC compared with tissue from *Dhcr7*$^{+/-}$ and *Dhcr7*$^{+/+}$ mice. 7-DHC accounted for 58% of total sterols, consistent with previously published elevated sterol levels for other tissues of this mouse model (Wassif et al., 2001). In *Sc5d*$^{-/-}$ embryos, lathosterol accumulates and is the major sterol present in tissues. Similar to the SLOS model, the lathosterol model also showed severely diminished cholesterol content and markedly increased lathosterol levels compared with the background amounts found in normal mice (Fig. 1C).

Cholesterol deficiency alters number and morphology of DCGs

Since cholesterol constitutes 70% of vesicular membrane lipids

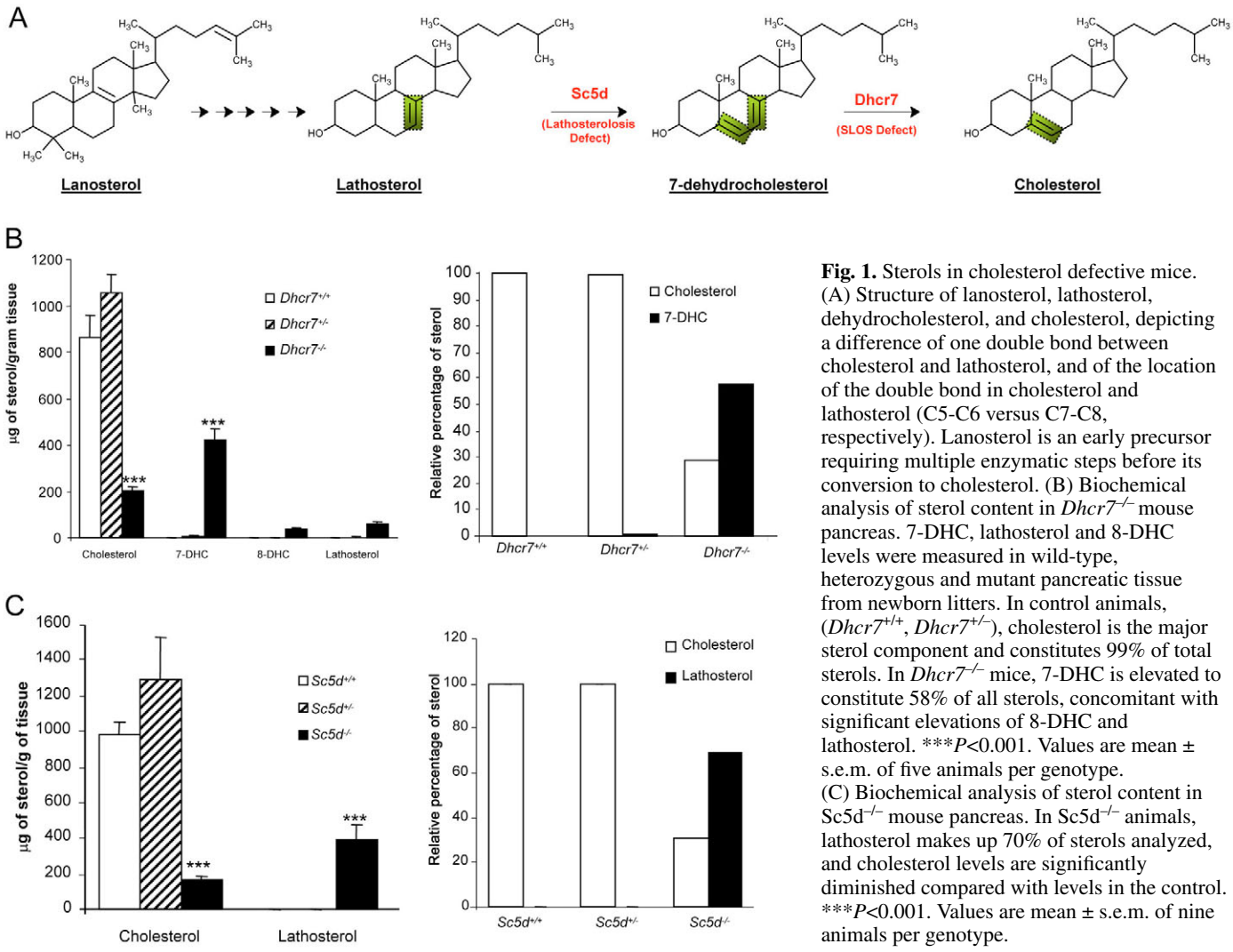

Fig. 1. Sterols in cholesterol defective mice. (A) Structure of lanosterol, lathosterol, dehydrocholesterol, and cholesterol, depicting a difference of one double bond between cholesterol and lathosterol, and of the location of the double bond in cholesterol and lathosterol (C5-C6 versus C7-C8, respectively). Lanosterol is an early precursor requiring multiple enzymatic steps before its conversion to cholesterol. (B) Biochemical analysis of sterol content in *Dhcr7*$^{-/-}$ mouse pancreas. 7-DHC, lathosterol and 8-DHC levels were measured in wild-type, heterozygous and mutant pancreatic tissue from newborn litters. In control animals, (*Dhcr7*$^{+/+}$, *Dhcr7*$^{+/-}$), cholesterol is the major sterol component and constitutes 99% of total sterols. In *Dhcr7*$^{-/-}$ mice, 7-DHC is elevated to constitute 58% of all sterols, concomitant with significant elevations of 8-DHC and lathosterol. ***P<0.001. Values are mean ± s.e.m. of five animals per genotype. (C) Biochemical analysis of sterol content in Sc5d$^{-/-}$ mouse pancreas. In Sc5d$^{-/-}$ animals, lathosterol makes up 70% of sterols analyzed, and cholesterol levels are significantly diminished compared with levels in the control. ***P<0.001. Values are mean ± s.e.m. of nine animals per genotype.

Journal of Cell Science

and has been shown to affect formation of dense core granules (DCGs) in endocrine cell lines in vitro (Dhanvantari and Loh, 2000; Wang et al., 2000), we reasoned that impaired cholesterol synthesis in vivo would result in defective granule formation. At the light and electron microscopic (EM) levels, compared with the normal dense core granule-packed exocrine pancreas in wild-type (WT) animals (Fig. 2A,C), certain areas of the SLOS pancreas were devoid of electron-dense cores (Fig. 2B). Instead, primarily light granular material and fused or unpinched vesicles were observed at the EM level (Fig. 2D-E).

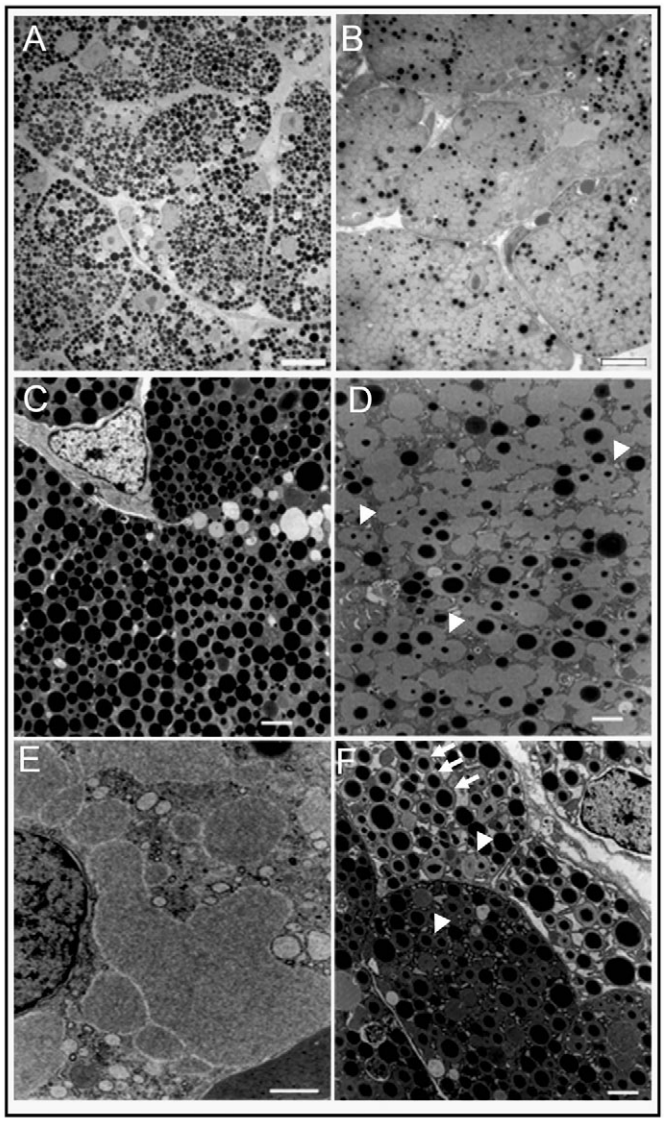

Fig. 2. Pancreas and secretory granule phenotype in *Dhcr7*$^{-/-}$ mice at P_0. Light images of thick sections (A-B) of pancreas show markedly decreased presence of dense core granules in sections of mutant pancreatic tissue (B), compared with numerous granules in *Dhcr7*$^{+/+}$ mice (A). Electron microscopic analysis of normal exocrine granules reveal membrane-bound vesicles 0.05-1.5 μm in diameter filled with electron-dense granular material (C). In *Dhcr7*$^{-/-}$ animals, abnormal profiles include vesicles with condensed material surrounded by a light halo bound by membrane (F, arrows), fused vesicles (D,F, arrowheads), or light granular material that failed to form vesicular shaped structures altogether (E). Bars, 10 μm (A-B); 1 μm (C-F).

Some abnormal granules with a large halo around the dense core were also present (Fig. 2F). By comparison, in lathosterolosis mice, granules were sparsely distributed in the exocrine pancreatic tissue (Fig. 3B), compared with the distribution in the WT animal (Fig. 3A). Additional features

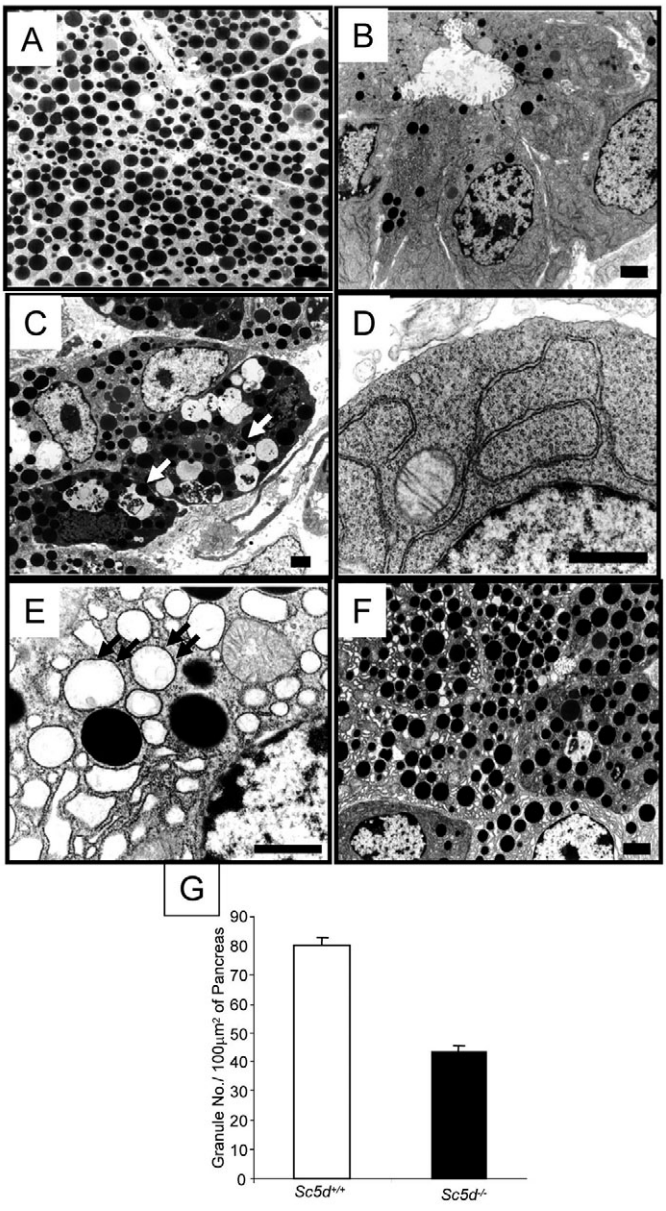

Fig. 3. Exocrine pancreas and secretory granule morphology in *Sc5d*$^{-/-}$ mice (lathosterolosis model) at E18.5. (A,B) *Sc5d*$^{-/-}$ animals consistently show a marked reduction in the number of dense core granules. In addition, many aberrant morphological profiles were evident: (C) large phagocytic structures with features of late endosomes or lysosomes engulfing cellular debris and granular material (arrows); (D) complete absence of dense core vesicles, and an abundance of ribosomal structures and rough ER; (E) enlarged ER (arrows). (F) A few areas have dense core vesicles similar to *Sc5d*$^{+/+}$ (WT), interspersed with profiles of enlarged ER. (G) Quantitative analysis of granule number in lathosterolosis mouse model. *Sc5d*$^{+/+}$ and *Sc5d*$^{-/-}$ groups contain four animals each. Ten different areas of each pancreas were imaged at low EM magnification (3150×) and counted. Bars, 2 μm (A-C,F); 1 μm (D-E).

prominent in the lathosterol mouse were enrichment in late-endosomal/lysosomal structures (Fig. 3C), ribosomal-like material (Fig. 3D), and enlarged ER (Fig. 3E). In some cases, normal granules were evident (Fig. 3F), but the size of the granules in lathosterolosis were often larger (Fig. 8C), and were 50% fewer in number than in WT animals (Fig. 3G, Fig. 8C).

The number and morphology of dense-core zymogen granules residing in exocrine cells of pancreatic acinar clusters also were quantitatively analyzed for the SLOS phenotype (Fig. 4). Mature granules were defined as having an electron-dense core that fills the entire membrane-delimited vesicular organelle. Aberrant non-dense core granular structures or membrane bound vesicles with partial dense cores were classified into the 'immature' category. In addition, because of the fused phenotype observed in SLOS mice, one granule was defined as being at least 75-100% spherically complete with a diameter greater than 0.05 μm. Granules were counted and expressed as the number of granules per 100 μm^2 of cytoplasmic area. As shown in Fig. 4, SLOS exocrine pancreas had 51±2.2 granules per 100 μm^2 of cytoplasmic area versus 73±3.2 in controls. Of the granules present in SLOS mice, 65% had an immature morphology, whereas this phenotype was only found in 31% of controls with nearly 70% of granules having a mature phenotype. Decreased granule formation was also observed in lathosterolosis mice (Fig. 3G). These animals exhibited a 45% decrease in total granule number.

Cholesterol deficiency alters secretory function of DCGs

α-amylase, a resident zymogen granule protein, is secreted in a regulated manner from acinar cells (Ohnishi et al., 1997; Schneider et al., 1997; Wang et al., 2004). Its regulated secretion might be impacted by the cholesterol deficiency causing malformation of secretory granules. We determined whether the observed abnormal morphology had an effect on the synthesis, expression and secretion of α-amylase in SLOS mice. Biochemically, there was no significant change in expression of α-amylase in control and SLOS tissues (Fig. 5A,B), however, levels of enzymatic activity were significantly elevated by 25% in blood serum of SLOS mice compared with control animals (Fig. 5C). This finding implied that the α-

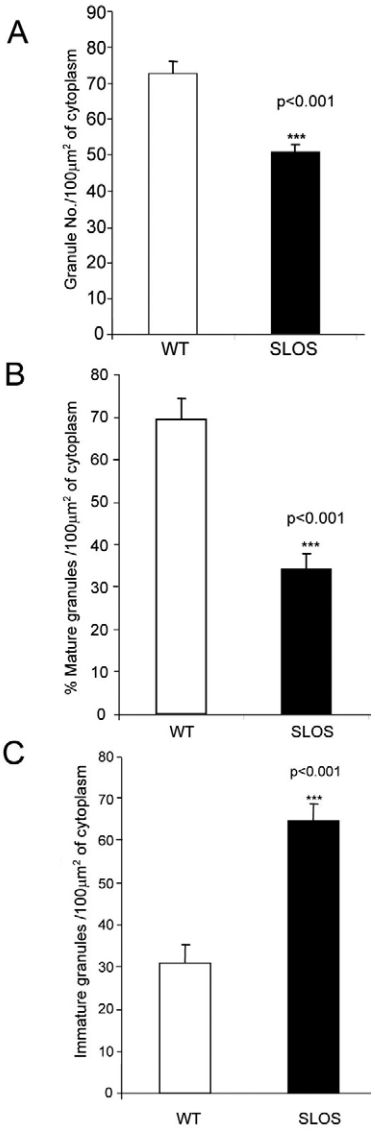

Fig. 4. Quantitative analysis of secretory granule morphology in pancreas. SLOS animals exhibit a 30% decrease in total granule number (A), a 60% decrease in the number of granules with mature morphology (B), and a 55% increase in granules with immature morphology (C). Mature is defined as round vesicles with a membrane bound dense core and no light granular halo. Immature is defined as all other morphologies including 'empty' granules. 10 images were analyzed per animal, at 3150X magnification, representative of each area within a section of pancreas. Each group represents the mean ± s.e.m. of four or five animals. ***P<0.001 compared with counts in the wild-type animals.

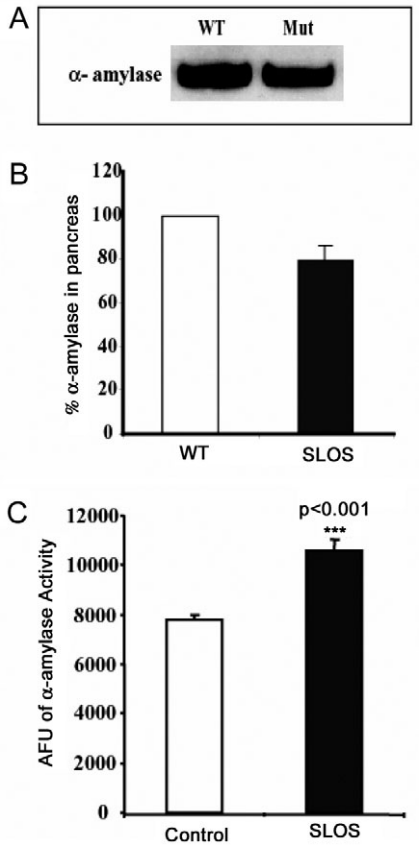

Fig. 5. Fate of proteins within the regulated secretory pathway in SLOS mice. (A) In vivo expression of α-amylase was analyzed by western blot of protein from whole pancreas of newborn SLOS littermates. (B) Quantification of bands shows abundant presence of α-amylase in both WT and SLOS mutants, with SLOS tissues exhibiting a 15% decrease in accumulation at steady state. (C) Plasma levels of α-amylase activity in blood. Activity was significantly elevated by 25% (***P<0.001) in circulating blood serum of SLOS mice compared with the level in WT serum. Values are mean ± s.e.m. of five animals from each group.

amylase present in tissues was secreted in a constitutive manner in SLOS mice, as opposed to the regulated pathway in controls. Furthermore, SLOS cells incorporated 50% less [^{35}S]Met into newly synthesized α-amylase, indicative of a reduction of synthetic machinery, compared with normal pancreatic cells (Fig. 6A). To test whether the cells had an intrinsic defective secretory mechanism, we used primary acinar cell cultures stimulated with carbachol, a cholinergic agonist, and assayed the stimulated release of α-amylase. Fig. 6B shows there was no detectable basal release (B) of α-amylase in control mice, but upon stimulation (S1), they exhibited a robust response. By contrast, SLOS pancreatic cells showed no stimulated secretion of α-amylase during S1, but a small amount was secreted during S2 (Fig. 6B). This is because DCGs were not formed in *Dhcr7*$^{-/-}$ pancreatic cells when grown in cholesterol-depleted medium (Fig. 6C, middle panel). However, when grown in serum-containing medium, primary cultures of SLOS cells regained their phenotype and were able to generate DCGs (Fig. 6C, right panel). Furthermore, these cells exhibited the ability to package DCG proteins and transport DCGs to the periphery as evidenced by the characteristic punctate staining of the granule marker, chromogranin A (CgA), similar to *Dhcr7*$^{+/+}$ cells (Fig. 6D, left vs right panel). This phenotype was absent in *Dhcr7*$^{-/-}$ cells grown in delipidated medium (Fig. 6D, middle panel). To test whether cholesterol alone was sufficient to induce granule formation, exocrine cells were incubated with either cholesterol or 7-DHC, and probed for CgA expression. *Dhcr7*$^{-/-}$ cells supplemented with cholesterol (Fig. 6E, bottom left) exhibited a pattern consistent with *Dhcr7*$^{+/+}$ cells (Fig. 6D,

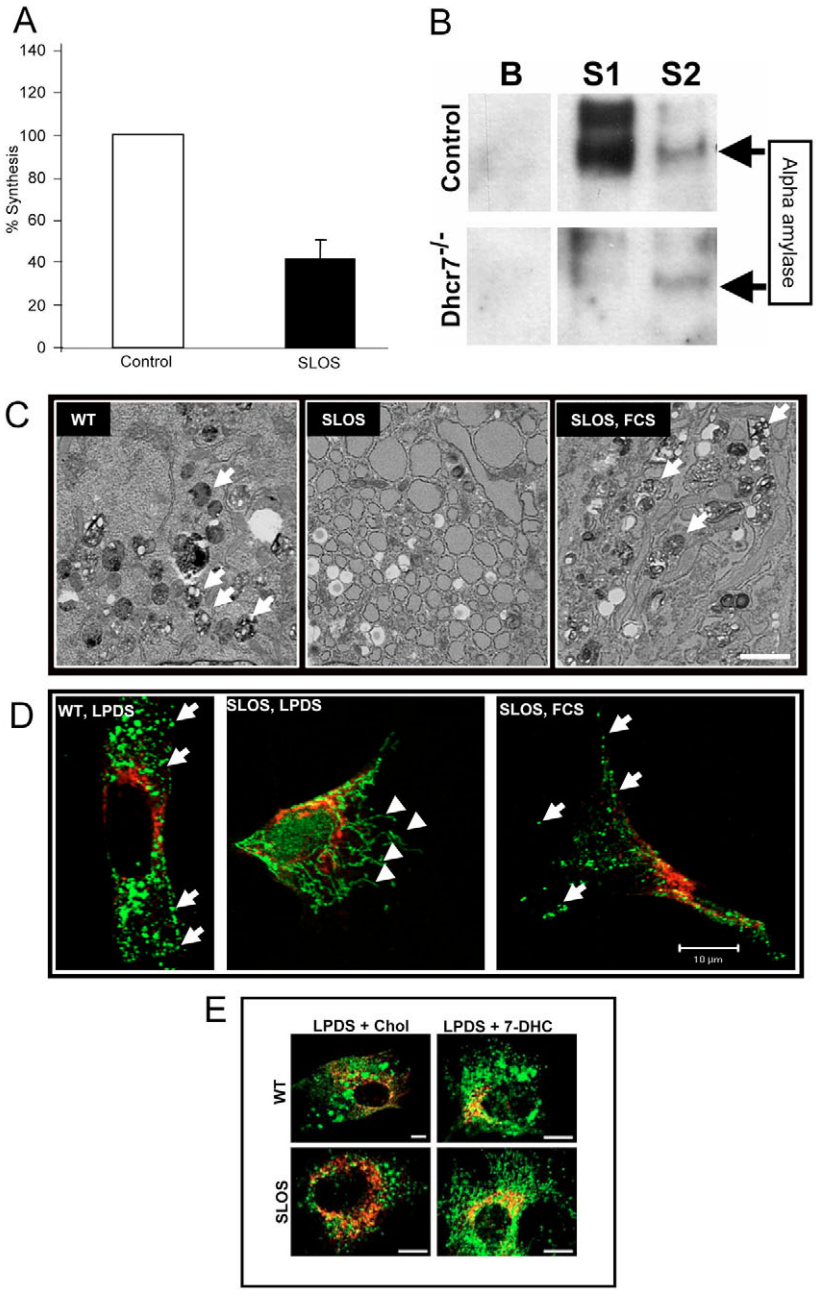

Fig. 6. Synthesis and secretion of α-amylase in cultured exocrine cells, and rescue of RSP. (A) Cells were pulse labeled for 30 minutes with [^{35}S]methionine. Cell lysates were harvested and immunoprecipitated with anti-α-amylase. Average synthesis in control animals was normalized to total CPM and defined as 100%. Values reported are the mean % CPM relative to control ±s.e.m. (B) Western blot analysis of α-amylase secreted in cultured pancreatic cells. Primary exocrine cells were equilibrated in basal media, and then a 1 hour basal secretion was collected. They were then stimulated with secretagogues for four 1-hour periods. B, basal release. S1 and S2, secretion during the third and fourth hour of stimulation, respectively. No secretion was evident during the first and second hour. (C) WT (left) and SLOS (middle and right) cells were cultured for 5.5 days in delipidated serum (LPDS) or fetal calf serum (FCS) and processed for electron microscopy. In the absence of lipid-containing serum, tubular profiles of ER-like structures were evident in SLOS (arrowheads), however when grown in the presence of lipid-containing FCS, electron dense granular vesicles were detected (arrows). (D) WT (left) and SLOS (middle and right) cells were cultured as in C, and probed for immunoreactivity to antibodies against the regulated secretory granule protein marker, CgA (green) or the Golgi marker p115 (red). In LPDS-containing media, CgA was localized to tubular profiles (arrowheads) of SLOS cells whereas when grown in the presence of FCS, they exhibited punctate vesicular structures (arrows), consistent with CgA localization to the RSP in controls. (E) In WT cells (top panels), vesicular staining of CgA (green) was detected upon addition of either cholesterol alone (left) or 7-DHC alone (right) to LPDS medium. In SLOS (bottom panels), vesicular patterns of CgA staining (green) were evident only if cholesterol (left) but not 7-DHC alone (right) was added to LPDS-medium. In the presence of 7-DHC, cells had numerous tubular profiles. Red, anti-p115. Bars, 2 μm (C); 10 μm (D,E).

left and 6E, top) or *Dhcr7*$^{-/-}$cells grown in fetal calf serum (Fig. 6D, right). However, when cells were exposed to 7-DHC (Fig. 6E, bottom right), the staining pattern was no different than untreated *Dhcr7*$^{-/-}$ cells grown in LPDS (Fig. 6D, middle).

DCG biogenesis defect is also in endocrine tissues

To identify the DCG defect in the cholesterol deficiency models, we initially used acinar cells of the exocrine pancreas because they contain large vesicles which facilitated quantification of the phenotypic defect. However, it was important to verify that the cholesterol defect also affects the formation of DCGs in neuroendocrine and endocrine tissues. We therefore analyzed the anterior pituitary (Fig. 7A and 7B), the adrenal medulla (Fig. 7C,D), and the endocrine pancreas (Fig. 7E,F) of Sc5d$^{-/-}$ mice. Compared with controls (Fig. 7A,C,E), the deficiency of granule number was recapitulated in these hormone-secreting cells from Sc5d$^{-/-}$ where dense core granules were either absent altogether or severely diminished (Fig. 7B,D,F).

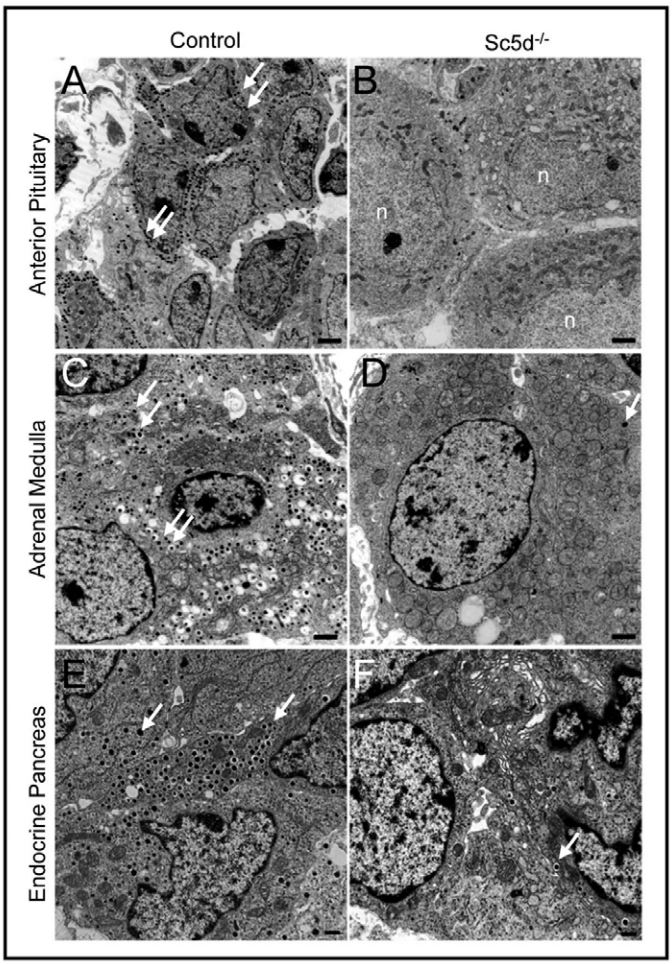

Fig. 7. Dense core granule formation in endocrine tissues of *Sc5d*$^{-/-}$ mice. At E18.5, DCGs are plentiful in the anterior pituitary (A), adrenal medulla (C) and endocrine pancreas (E) of control mice, whereas mice homozygous for the Sc5d mutation show absent or severely reduced presence of electron-dense granules (arrows) in equivalent regions of tissues (B,D,F). n, nucleus. Bars, 1 μm (A-B); 2 μm (C-D); 500 nm (E-F).

Sterol substitution alters membrane physical properties

To determine whether the morphological and biochemical changes observed are related to modification of membrane elasticity owing to either depletion of cholesterol or replacement with 7-DHC or lathosterol, we measured the changes in membrane behavior in vitro, in the presence of each sterol. Embedded sterols affect the distribution of forces within biomembranes and introduce bending stress (Harries and Ben-Shaul, 1997; Petrache et al., 2000; Rand et al., 1990). This energetic shift is most efficiently measured by two elasticity parameters: the monolayer bending rigidity, K_C^{mono}, and the monolayer intrinsic curvature $1/R_0$ (Helfrich, 1978; Seddon, 1990). In its simplest form, the energy cost of bending a monolayer away from R_0 is

$$F^{m}_{elastic}(R) \approx \frac{1}{2} K_C^{mono} \left(\frac{1}{R} - \frac{1}{R_0} \right)^2 , \qquad (1)$$

where K_C^{mono} represents the energy needed to flatten a spontaneously curved monolayer of area $2R_0^2$. Constrained within a bilayer geometry, apposed monolayers confer an overall membrane bending rigidity, K_C, which depends on both K_C^{mono} and R_0. For many bilayer-forming phospholipids, K_C is in the order of 12 kcal/mol (Petrache et al., 1998a; Rawicz et al., 2000). We measured changes in K_C using lamellar dimyristoylphosphatidylcholine (DMPC) and in R_0 using dioleoylphosphatidylethanolamine (DOPE).

When two thermally fluctuating membranes are brought nearby, the mutual restriction of bending fluctuation generates a repulsive force (Helfrich, 1978). X-ray measurements of interbilayer equilibrium spacing (D_W) under applied osmotic stress provides this repulsion interaction (Eq. 2) and the membrane bending rigidity, K_C (Petrache et al., 1998a; Petrache et al., 1998b):

$$F_{fluc}(D_W,T) = \left(\frac{k_B T}{2\pi} \right)^2 \frac{1}{K_C \sigma^2} . \qquad (2)$$

Here k_B is the Boltzmann constant (a fundamental thermodynamic parameter) equal to 1.38×10^{-23} J/K. It quantifies molecular thermal energy k_BT which at 35°C (T ~308K) is about 0.6 kcal/mol. σ^2 in the denominator represents the mean-square amplitude of membrane thermal undulations. In Fig. 8A, we show bending rigidities obtained from the analysis of interbilayer interactions (Eq. 2) of bilayer-forming DMPC. As seen by the lower energy needed to push fluctuating membranes closer, it required more energy to bend cholesterol-containing membranes. At 35°C, addition of 30 mol% cholesterol increased membrane rigidity by ~100% (11.6 vs 23.9 kcal/mol). However, membrane rigidity increased less for the other sterols, in the order: cholesterol>lathosterol>7-DHC. When sterols were added to the non-bilayer-forming DOPE, the lattice spacing of the highly curved, inverse hexagonal phase was modified. Fig. 8B shows a shift of the X-ray scattering peaks to lower q-values, corresponding to an increase in the monolayer radius of curvature in the order cholesterol<lathosterol<7-DHC. In addition to changes in bending rigidity, the elastic energy owing to curvature of the membrane also changed by 1.2 and 1.8 kcal/mol upon substitution with lathosterol or 7-DHC, respectively. These differences in bending rigidity and curvature correlate with the

possible elastic deformation observed in morphologies of SLOS and lathosterol granules in Figs 2 and 3.

To confirm whether these results were consistent with the phenotype observed in vivo, we measured the volume of acinar cell granules of the *Dhcr7*$^{-/-}$ and *Sc5d*$^{-/-}$ disease models and binned them according to size (Fig. 8C). Metamorph analysis of the images indicated a cluster of 70% of all normal granules within the range of 0.05 to 0.6 μm^2, whereas the majority of granules from the lathosterolosis model (55%) were $\geqslant$0.6 μm^2 and were observed to be as large as 5.0 μm^2, a size never observed for controls. This indicates that the excess lathosterol in the membrane of lathosterolosis mouse granules (Fig. 1C) contributes to the formation of enlarged granules (Fig. 8C), probably because of the excess elasticity conferred to membranes by lathosterol compared with cholesterol as revealed in studies using artificial membranes (Fig. 8A,B). SLOS animals were not included in this analysis because circular granule structures often failed to form, and many immature profiles were evident, causing difficulties in obtaining accurate values for dense core volumes.

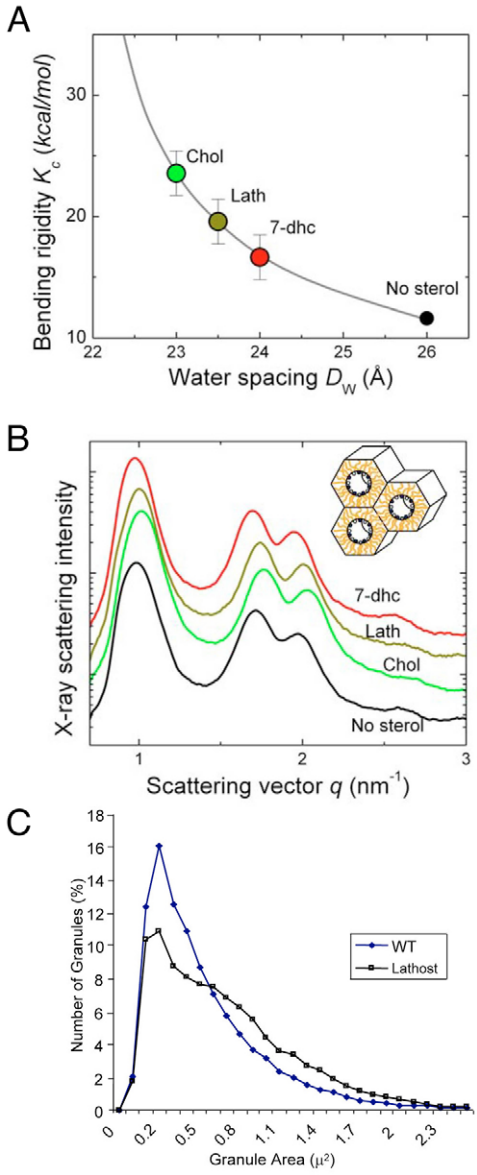

Fig. 8. Impact of abnormal sterol expression on membrane curvature. (A) Membrane bending rigidity K_C obtained from measured interactions of multilamellar DMPC vesicles at 35°C containing 30 mol% sterols. The importance of double-bond location in the sterol ring is illustrated, with cholesterol the most efficient at enhancing membrane rigidity. (B) X-ray scattering of highly curved, inverse hexagonal phase DOPE/30mol% sterol mixtures. The shift of scattering peaks with sterol type corresponds to changes in the radius of curvature of bent DOPE monolayers with the smallest values measured for cholesterol and the largest for 7-DHC. Depletion of cholesterol or replacement with 7-DHC or lathosterol modifies the distribution of forces (bending stress) within biomembranes contributing to cellular morphological changes. (C) Distribution of granule sizes in the lathosterol model. 30 images from each of three animals were analyzed. Granule areas are distributed over a greater range compared with the normal WT range.

Discussion

Regulated, stimulus-dependent secretion via the exocytosis of dense core granule content provides a mechanism for controlling delivery of hormones, enzymes, neuropeptides, and neurotransmitters to a target cell or organ in a timely and quantified manner (Burgoyne and Morgan, 2003; Loh et al., 2004; Lou et al., 2005). In this study, we have investigated the contributions of cholesterol, 7-DHC and lathosterol to granule biogenesis and regulated secretion in exocrine and endocrine tissues of mouse models of SLOS and lathosterolosis. We report here that cholesterol is necessary for the correct formation of granules in vivo. In the formation of regulated secretory vesicles in animals with inborn errors of cholesterol synthesis, cholesterol cannot be substituted by other lipids with structural similarity. We also show deregulated secretion of cargo in acinar cells of the exocrine pancreas, owing to the absence of cholesterol, which suggests impairment of cellular function.

It has been reported that cholesterol-rich lipid rafts in the TGN serve as the platform for DCG biogenesis (Loh et al., 2004). This model is supported by the finding that cholesterol makes up approximately 70% of the lipids in vesicular membranes (Dhanvantari and Loh, 2000), and targeting of proteins to vesicles in the RSP is cholesterol and lipid raft dependent (Wang et al., 2000; Zhang et al., 2003). In disease models where cholesterol is lacking, granule formation decreases by 30% in newborn 7-DHC mutants and by 45% in Sc5d mutants (Fig. 3G and Fig. 4). In each animal model, residual cholesterol corresponding to ~20% of normal levels was present in the pancreas as reported in other tissues (Krakowiak et al., 2003; Wassif et al., 2001). Since the animals are feeding impaired, we assume this cholesterol to be maternally derived, and may account for the formation of some vesicles. Upon extraction of cholesterol and synthetic inhibition of its biosynthesis, vesicle formation was prevented and dense core granule proteins were no longer associated with lipid rafts in neuroendocrine cell lines (Dhanvantari and Loh, 2000; Wang et al., 2000). This phenotype was rescued both in cell lines (Dhanvantari and Loh, 2000; Wang et al., 2000) and in primary cultures of SLOS cells, which formed granules upon addition of exogenous cholesterol to the cell mixture (Fig. 6C-E). In contrast to the tubular appearance of the DCG protein, CgA, in *Dhcr7*$^{-/-}$ pancreatic cells, CgA distribution in cholesterol-rescued *Dhcr7*$^{-/-}$ cells was punctate and localized

Journal of Cell Science

to the periphery of the cell in the classic pattern of vesicular-packaged granule proteins. This establishes that the granule formation defect is a consequence of the biochemical perturbation. This is consistent with the vesicular-trafficking defect observed in SLOS, Niemann-Pick disease type C and other diseases where cholesterol and/or glycosphingolipid metabolism is impaired (Gondré-Lewis et al., 2003; Wassif et al., 2002).

Since the discovery that 7-DHC is elevated in SLOS, and lathosterol in lathosterolosis, a major question has been whether the developmental, cellular and biochemical defects are due to the lack of cholesterol or to the increase in precursor levels. Recent evidence suggests that 7-DHC can form detergent-resistant microdomains in liposomes in vitro and in animal models of SLOS (Keller et al., 2004). In fact, natural sterols such as ergosterol and 7-DHC reportedly form more stable domains and lipid-lipid interactions than cholesterol (Xu et al., 2001), although native cholesterol in microdomains is essential for efficient membrane fusion of secretory vesicles (Churchward et al., 2005). Indeed, we also detected no change in the incorporation of lipid raft proteins, flotilin and Cav-1 into detergent-resistant microdomains in flotation assays performed on diseased and normal brain (data not shown). However, analysis of lipid raft components in brain by 2-D gel electrophoresis revealed several proteins or proteomes that are differentially regulated in the AY9944 drug-induced model of SLOS (Keller et al., 2004). Therefore, it is possible that certain proteins involved in the budding process or which are normally recruited into DCGs are not routed to TGN membrane microdomains in *Sc5d*$^{-/-}$ and *Dhcr7*$^{-/-}$, and thus induce increased numbers of protein-containing ribosomal-like structures, or enlarged ER, pervasive in these models (Figs 2 and 3).

When cholesterol is incorporated into membranes, its sterol rings interact with the phospholipid groups to yield the characteristic curvature and fluidity necessary for vesicular budding (Bloom et al., 1991; Henriksen et al., 2004; Martinez et al., 2004; Méléard et al., 1997).

We hypothesize that in inborn errors of cholesterol synthesis, where 7-DHC or lathosterol are highly elevated, the abnormal presence of these sterols can change the lipid interaction properties and characteristics of the membrane (Bloom et al., 1991). In the case of increased lathosterol, granules are either not formed or are far greater in diameter than normal (Fig. 3). In SLOS, excess 7-DHC yields immature or fused granular structures. Indeed, our quantitative X-ray measurements of membrane interactions and fluctuations show that sterols behave differently in reconstituted membranes, increasing membrane rigidity in the order 7-DHC<lathosterol< cholesterol. Cholesterol makes the most compact membrane bilayers and, therefore, displays higher membrane rigidity (Fig. 8A). Furthermore, the intrinsic radius of curvature of non-lamellar structures is greatest for 7-DHC and smallest for cholesterol, whereas lathosterol is intermediate (Fig. 8B). Thus, consistent with observations in vivo, cholesterol is more likely to maintain the curvature of vesicles than its precursors, as demonstrated by the biophysics of sterol incorporation in artificial membranes. One explanation for the morphological phenotype observed at the electron microscopic level is that cholesterol may be critical for the pinching off of vesicles at the TGN through its facilitation of membrane fusion (Churchward et al., 2005), and for incorporation of resident proteins in the zymogen-, endocrine- or neuropeptide-containing granule. Since the lipid environment necessary for recruitment of proteins to the regulated pathway is missing, these proteins may be misrouted and secreted constitutively, or sequestered into other parts of the Golgi and in lysosomes (Loh et al., 2002). Future experiments will address the ratiometric contribution of sterol combinations to the lipid bilayer, to more closely approximate the status in cholesterol-deficiency diseases.

Primary acinar cells from *Dhcr7*$^{-/-}$ mice display defective regulated secretion when stimulated. Similarly, in vivo, amylase activity was significantly elevated in the plasma of *Dhcr7*$^{-/-}$ animals compared with normal animals. Although we cannot rule out leaky membranes or cell death, our studies on primary exocrine pancreatic cells suggest shunting of the amylase into an unregulated pathway for secretion. Information on pancreatic histology and pathology in SLOS patients is limited. Pancreatic islet hyperplasia with atypical giant cells and enlarged hyperchromatic nuclei have been reported (Cherstvoy et al., 1984; Kohler, 1983; Lachman et al., 1991; Ness et al., 1997). No information is available regarding the status of pancreatic dense core granules in SLOS patients. Given the finding of elevated amylase in serum from *Dhcr7*$^{-/-}$ pups, we evaluated serum amylase and lipase levels in a series of 45 SLOS patients (age 9 months to 28 years, physical severity scores 6-50). Serum lipase levels were normal, and an elevated amylase level was only observed in one patient. In contrast to the *Dhcr7*$^{-/-}$ pups, the SLOS patients in this series all are on dietary cholesterol supplementation, and have much lower plasma 7-DHC:total sterol fractions. We are currently unable to test the effects of exogenous administration of cholesterol in the secretory cells of mice in vivo, as the animal models in this study only live for 1 day. However, granule formation was rescued in isolated SLOS cells grown in a cholesterol-rich environment (Fig. 6), consistent with the phenotype of patients administered exogenous cholesterol. Growth failure and feeding intolerance is frequently observed in SLOS infants (Kelley and Hennekam, 2000). The observation of abnormalities of pancreatic dense granule formation in the SLOS mouse model suggests that SLOS patients with failure to thrive should be evaluated for exocrine pancreatic insufficiency.

In this study using mouse models of cholesterol deficiency diseases, we demonstrated that cholesterol is required for the formation and maturation of secretory vesicles in vivo. When sterols other than cholesterol are present, the integrity of the membrane of large dense core granules is compromised, and this results in the absence or malformation of vesicles. With quantitative measurements of membrane sterol X-ray-scattering characteristics, we correlated decreased bending rigidity and intrinsic curvature with the lack of cholesterol and increased granule size in SLOS and lathosterolosis. The elucidation of a mechanism for cholesterol-mediated vesicular budding in normal cells has revealed new insights into the pathophysiology of cholesterol-deficiency diseases. Our studies provide evidence that granule formation in both exocrine and endocrine tissues are affected by cholesterol deficiency, which probably accounts for multiple physiological deficits observed in SLOS and lathosterol patients.

Journal of Cell Science

Materials and Methods

Antibodies

The rabbit polyclonal antibody against α-amylase was a kind gift from Bruce Baum (NIDCR, National Institutes of Health). Anti-CgA polyclonal IgG was previously described (Arnaoutova et al., 2003). Anti-p115 mouse IgG is from BD Transduction Laboratories (San Jose, CA). Alexa Fluor 488- and Alexa Fluor 546-labeled rabbit IgG fraction was obtained from Molecular Probes (Carlsbad, CA). HRP-conjugated anti-rabbit IgG was purchased from Amersham Biosciences (Piscataway, NJ).

Animals

Dhcr7$^{-/-}$ mice were generated by targeted disruption of the Dhcr7 gene as previously described (Wassif et al., 2001). *Dhcr7*$^{-/-}$ mice live no more than 24 hours after birth, and were therefore used at postnatal day 0 (P_0). All experiments routinely included littermate controls and represent animals from many litters. *Sc5d*$^{-/-}$ were generated by disruption of the lathosterol 5-desaturase gene (Sc5d) as described (Krakowiak et al., 2003). These mice are stillborn, and are acquired and used at embryonic day (E)18. Experimental protocols were approved and carried out in accordance with the Animal Care and Use Committee of the National Institutes of Health.

Genotyping and sterol analysis

Tail biopsies of newborns generated from *Dhcr7*$^{+/-}$ or *Sc5d*$^{+/-}$ intercross matings were genotyped as previously described (Krakowiak et al., 2003; Wassif et al., 2001). Sterols were extracted from the pancreas of 15 newborn Dhcr7 (5 *Dhcr7*$^{+/+}$, 5 *Dhcr7*$^{+/-}$, 5 *Dhcr7*$^{-/-}$) and 20 Sc5d (6 *Sc5d*$^{+/-}$, 6 *Sc5d*$^{+/-}$, 8 *Dhcr7*$^{-/-}$) littermates and analyzed by gas chromatography and/or mass spectrometry as published (Wassif et al., 2001).

Electron microscopy

Cell culture monolayers were washed in phosphate buffer and fixed in 2.5% glutaraldehyde for 4 hours. Tissue samples were quickly excised from E18 or newborn animals and fixed in 2.5% glutaraldehyde for 16 hours in preparation for transmission electron microscopy. Both types of samples were then washed three times for 5 minutes each in phosphate buffer and post-fixed in 1% osmium tetroxide for 1-2 hours, followed by four 5-minute washes in deionized H_2O. Tissues were stained en bloc with 2% uranyl acetate for 1 hour, and then dehydrated twice for 5 minutes each in 70, 80 and 90% ethanol; and then three times in 100% ethanol for 5 minutes. The ethanol dehydration was followed by three 5-minute incubations in propylene oxide. Tissues were infiltrated for 30-60 minutes each with 1:1, 1:2, and 1:3 ratio of propylene oxide:Spurr's plastic resin, followed by pure Spurr's resin for 30-60 minutes. Tissues were then embedded in fresh plastic and placed in a 70°C oven for polymerization. Sections were cut at a thickness of 600-800 Å and mounted on copper grids, followed by staining in lead citrate for 1.5 minutes. The stained grids were examined on a Zeiss EM 10 CA or Jeol 1010 transmission electron microscope. Tissue processing was performed by JFE Enterprises, Brookeville, MD.

Primary pancreatic cultures from SLOS mice

Primary acinar cells in culture were established using modifications of a previously described protocol (Kurup and Bhonde, 2002). Newborn P_0 animals from SLOS heterozygous (*Dhcr7*$^{+/-}$) matings were quickly decapitated with a razor blade, the pancreas excised and rinsed several times in 0.01% soybean trypsin inhibitor (STI). Tissue was dissociated in phosphate-buffered saline (PBS) containing 0.02% trypsin and 0.25% EDTA at 37°C for 5 minutes, centrifuged at 800 ***g*** for 2 minutes and dissociation was terminated with F12K medium containing 20% fetal calf serum (FCS), 5 mg/ml bovine serum albumin (BSA), 0.1 mg/ml soybean trypsin inhibitor (STI) and 1% penicillin/streptozotocin (Pen/Strep). Tissue was then placed in a digestive solution containing 1 mg/ml collagenase P, 0.2 mg/ml BSA at 37°C for 30 minutes, then centrifuged at 800 ***g*** for 2 minutes. Cells were resuspended in F12K medium containing 10% FCS and Pen/Strep, and rinsed twice. Cells from each individual pancreas were plated in three 35-mm dishes in F12K containing 20% lipoprotein-deficient serum (LPDS) and 5 mg/ml BSA, 0.1 mg/ml STI, 1% Pen/Strep and allowed to adhere on collagen-coated dishes for 4 days, after which the medium was changed every 3-4 days.

Phenotype rescue

Cells were plated and maintained in LPDS- or FCS-containing media for 5-6 days. Sterols were introduced into cultures in accordance with published methods (Christian et al., 1997). 19.2 μl of a 50 mg/ml solution of cholesterol or 7-DHC in 1:1 chloroform:methanol was allowed to air dry, was mixed with 2.5 mM methyl-β-cyclodextran (MβCD) in F12K by vortex, sonicated for 1-3 minutes and incubated overnight in a shaking water bath at 37°C. Each 10:1, 2.5 mM MβCD:sterol solution was passed through a 0.45 μm filter before introduction into cells for 24 hours.

Synthesis assay and immunoprecipitation (IP)

Primary exocrine cultures were depleted of methionine by incubation in methionine-free DMEM for 30 minutes. Cells were then labeled for 30 minutes in methionine-free DMEM containing 100 μCi/ml [^{35}S]methionine, placed on ice and washed once with ice-cold PBS. Cells were scraped and lysed in the presence of 1% Triton X-100 in TNE buffer. Lysates were pre-cleared in 50 μl protein-A-Sepharose beads followed by immunoprecipitation (IP) overnight at 4°C with α-amylase antibody at a final dilution of 1:100. Immunoprecipitated α-amylase was captured on protein-A-Sepharose beads during a 1 hour incubation at 4°C, centrifuged at 2000 ***g***, and washed four times in wash buffer (1% TX-100, 50 mM Tris-HCl pH 7.4, 300 mM NaCl, 5 mM EDTA). The pellet was resuspended in SDS-containing loading buffer and beads were removed by boiling and centrifugation before loading on a 4-12% Novex Nupage gel (Invitrogen, Carlsbad, CA). Total CPM of cell lysates were determined pre- and post-IP. Some samples were precipitated with 20% TCA before IP to eliminate the contribution to total CPM of extraneously bound ^{35}S, but this procedure had no effect on the final percentage synthesis values. Radiolabeled α-amylase was detected both on film and by scanning densitometry on the STORM 860 autoradiography and analyzed with Molecular Dynamics ImageQuant 5.2 software. Controls were calculated as a fraction of total synthesis and normalized to 100%. Mutant values were calculated as a percentage of the control.

Secretion assay

Cells grown under the conditions described above were washed quickly with Hanks' balanced salt solution (HBSS), and incubated either three times for 30 minutes or twice for 1 hour with F12K medium for assessment of basal secretion. To stimulate cells, DMEM containing 50 mM KCl, 2 mM $BaCl_2$, 2×10^{-8} M carbachol was applied each hour for 4 hours. Medium was collected after each basal and stimulation incubation and used for western blot analysis.

Immunocytochemistry

Mutant and normal primary cultures grown on collagen-coated coverslips in the presence or absence of cholesterol for 5.5 days were washed in HBSS, and fixed in 4% paraformaldehyde for 30 minutes at room temperature, permeabilized with 0.1% Triton X-100 and blocked for 1 hour in 1% BSA. Cells were incubated in anti-chromogranin A (anti-CgA) rabbit IgG, and anti-p115 mouse IgG overnight at 4°C, washed and then probed with Alexa Fluor 546-conjugated goat-anti-mouse IgG and Alexa Fluor 488-conjugated goat anti-rabbit IgG. Coverslips were mounted onto slides with an aqueous mounting medium Gel/Mount (Biomeda Corp., Foster City, CA). Images were acquired on a Zeiss Axiovert 200 M inverted microscope using a 63× plan apochromat oil, 1.4 NA objective. FITC and Rhodamine were scanned with either an Argon ion laser, 30 mW or a Helium-Neon laser, 1 mW and detected with the appropriate filters. The system is equipped with a Zeiss LSM 5 acquisition software. Photoshop was used to generate montages with no further processing.

Western blot

Whole pancreas was removed from P_0 SLOS and control mice, and either flash-frozen for future use or immediately homogenized in TNE with 1% Triton X-100 and protease inhibitor, and subjected to three freeze/thaw cycles. After centrifugation at 2000 ***g*** for 10 minutes, the post-nuclear supernatant was removed, and protein content assayed using the Bradford method. Equivalent protein concentrations were loaded onto Nupage gels under reducing conditions and transferred onto nitrocellulose membrane. Membranes were incubated in 1:5000 dilution of α-amylase primary antibody followed by goat anti-rabbit IgG secondary antibody. Immunoreactivity was visualized with Supersignal West Dura solution (Pierce Biotechnology, Rockford, IL), and developed on Kodak film.

Plasma analysis

Blood samples were immediately retrieved from the trunk of decapitated animals with a pipette tip. Serum was separated from blood cells by spinning at 13,000 ***g*** in a microcentrifuge for 5 minutes at 4°C. Amylase activity from equivalent volumes of serum was analyzed based on the ability of amylase to cleave Bodipy-conjugated starch substrate and exposing the fluorescent molecule in the Enzchek amylase assay kit (Molecular Probes, Eugene, OR). Fluorescence intensities were read on the Synergy HT microplate reader (Bio-Tek Instruments, Winooski, VT).

Small-angle X-ray scattering (SAXS)

Highly purified (>99%) synthetic phospholipids, 1,2-dimyristoyl-*sn*-glycero-3-phosphocholine and 1,2-dioleoyl-*sn*-glycero-3-phosphoethanolamine (Avanti Polar Lipids, Alabaster, AL), were dissolved with appropriate amounts of sterols in chloroform and dried to a thin film under high vacuum. The lipid/sterol mixtures were then hydrated with purified water or high molecular weight (20 K) polyethylene glycol solutions with known concentrations and osmotic pressures. Samples with 7-DHC were prepared under argon with minimal exposure to ambient light. Samples were stored at –4°C before being X-rayed for 0.5-1 hour at 35°C with a fine-focus fixed copper anode X-ray source (Enraf-Nonius, Delft, The Netherlands). Sharp, uniform scattering rings were obtained indicative of sample homogeneity upon equilibration. Lattice spacings were recorded as a function of sterol content and applied osmotic pressure and analyzed in terms of interbilayer forces for lamellar structures and monolayer curvatures for inverse-hexagonal phases to obtain information on membrane-bending rigidities.

Journal of Cell Science

Statistical analysis

Data are expressed as mean ± s.e.m. Two-tailed analysis was performed by unpaired *t*-test.

We thank Jennifer Lippincott-Schwartz and Owen Rennert (National Institute of Child Health and Human Development, NIH) for critical reading of the manuscript and Bruce Baum (National Institute of Dental and Craniofacial Research, NIH) for the anti-α-amylase antibody. We also thank Chip Dye (Microscopy & Imaging Core, National Institute of Child health and Development, NIH) for assistance with imaging. The authors declare that they have no competing financial interests. This research was supported by the Intramural Research Program of the NICHD, NIH.

References

Arnaoutova, I., Smith, A. M., Coates, L. C., Sharpe, J. C., Dhanvantari, S., Snell, C. R., Birch, N. P. and Loh, Y. P. (2003). The prohormone processing enzyme PC3 is a lipid raft-associated transmembrane protein. *Biochemistry* **42**, 10445-10455.

Bloom, M., Evans, E. and Mouritsen, O. G. (1991). Physical properties of the fluid lipid-bilayer component of cell membranes – a perspective. *Q. Rev. Biophys.* **24**, 293-397.

Brunetti-Pierri, N., Corso, G., Rossi, M., Ferrari, P., Balli, F., Rivasi, F., Annunziata, I., Ballabio, A., Russo, A. D., Andria, G. et al. (2002). Lathosterolosis, a novel multiple-malformation/mental retardation syndrome due to deficiency of 3beta-hydroxysteroid-delta5-desaturase. *Am. J. Hum. Genet.* **71**, 952-958.

Burgoyne, R. D. and Morgan, A. (2003). Secretory granule exocytosis. *Physiol. Rev.* **83**, 581-632.

Cherstvoy, E. D., Lazjuk, G. I., Ostrovskaya, T. I., Shved, I. A., Kravtzova, G. I., Lurie, I. W. and Gerasimovich, A. I. (1984). The Smith-Lemli-Opitz syndrome. A detailed pathological study as a clue to a etiological heterogeneity. *Virchows Arch. A Pathol. Anat. Histopathol.* **404**, 413-425.

Christian, A. E., Haynes, M. P., Phillips, M. C. and Rothblat, G. H. (1997). Use of cyclodextrins for manipulating cellular cholesterol content. *J. Lipid Res.* **38**, 2264-2272.

Churchward, M. A., Rogasevskaia, T., Hofgen, J., Bau, J. and Coorssen, J. R. (2005). Cholesterol facilitates the native mechanism of Ca2+-triggered membrane fusion. *J. Cell Sci.* **118**, 4833-4848.

Dhanvantari, S. and Loh, Y. P. (2000). Lipid raft association of carboxypeptidase E is necessary for its function as a regulated secretory pathway sorting receptor. *J. Biol. Chem.* **275**, 29887-29893.

Gondré-Lewis, M. C., McGlynn, R. and Walkley, S. U. (2003). Cholesterol accumulation in NPC1-deficient neurons is ganglioside dependent. *Curr. Biol.* **13**, 1324-1329.

Harries, D. and Ben-Shaul, A. (1997). Conformational chain statistics in a model lipid bilayer: comparison between mean field and Monte Carlo calculations. *J. Chem. Phys.* **106**, 1609-1619.

Helfrich, W. (1978). Steric interaction of fluid membranes in multilayers systems. *Z. Naturforsch.* **33**, 305A-315A.

Henriksen, J., Rowat, A. C. and Ipsen, J. H. (2004). Vesicle fluctuation analysis of the effects of sterols on membrane bending rigidity. *Eur. Biophys. J.* **33**, 732-741.

Keller, P. and Simons, K. (1998). Cholesterol is required for surface transport of influenza virus hemagglutinin. *J. Cell Biol.* **140**, 1357-1367.

Keller, R. K., Arnold, T. P. and Fliesler, S. J. (2004). Formation of 7-dehydrocholesterol-containing membrane rafts in vitro and in vivo, with relevance to the Smith-Lemli-Opitz syndrome. *J. Lipid Res.* **45**, 347-355.

Kelley, R. I. and Hennekam, R. C. (2000). The Smith-Lemli-Opitz syndrome. *J. Med. Genet.* **37**, 321-335.

Kohler, H. G. (1983). Brief clinical report: familial neonatally lethal syndrome of hypoplastic left heart, absent pulmonary lobation, polydactyly, and talipes, probably Smith-Lemli-Opitz (RSH) syndrome. *Am. J. Med. Genet.* **14**, 423-428.

Krakowiak, P. A., Wassif, C. A., Kratz, L., Cozma, D., Kovarova, M., Harris, G., Grinberg, A., Yang, Y., Hunter, A. G., Tsokos, M. et al. (2003). Lathosterolosis: an inborn error of human and murine cholesterol synthesis due to lathosterol 5-desaturase deficiency. *Hum. Mol. Genet.* **12**, 1631-1641.

Kurup, S. and Bhonde, R. R. (2002). Analysis and optimization of nutritional set-up for murine pancreatic acinar cells. *Jop* **3**, 8-15.

Lachman, M. F., Wright, Y., Whiteman, D. A., Herson, V. and Greenstein, R. M. (1991). Brief clinical report: a 46,XY phenotypic female with Smith-Lemli-Opitz syndrome. *Clin. Genet.* **39**, 136-141.

Loh, Y. P., Maldonado, A., Zhang, C., Tam, W. H. and Cawley, N. (2002). Mechanism of sorting proopiomelanocortin and proenkephalin to the regulated secretory pathway of neuroendocrine cells. *Ann. N. Y. Acad. Sci.* **971**, 416-425.

Loh, Y. P., Kim, T., Rodriguez, Y. M. and Cawley, N. X. (2004). Secretory granule biogenesis and neuropeptide sorting to the regulated secretory pathway in neuroendocrine cells. *J. Mol. Neurosci.* **22**, 63-71.

Lou, H., Kim, S. K., Zaitsev, E., Snell, C. R., Lu, B. and Loh, Y. P. (2005). Sorting and activity-dependent secretion of BDNF require interaction of a specific motif with the sorting receptor carboxypeptidase e. *Neuron* **45**, 245-255.

Martinez, G. V., Dykstra, E. M., Lope-Piedrafita, S. and Brown, M. F. (2004). Lanosterol and cholesterol-induced variations in bilayer elasticity probed by H-2 NMR relaxation. *Langmuir* **20**, 1043-1046.

Méléard, P., Gerbeaud, C., Pott, T., Fernandez-Puente, L., Bivas, I., Mitov, M. D., Dufourcq, J. and Bothorel, P. (1997). Bending elasticities of model membranes: influences of temperature and sterol content. *Biophys. J.* **72**, 2616-2629.

Ness, G. C., Lopez, D., Borrego, O. and Gilbert-Barness, E. (1997). Increased expression of low-density lipoprotein receptors in a Smith-Lemli-Opitz infant with elevated bilirubin levels. *Am. J. Med. Genet.* **68**, 294-299.

Ohnishi, H., Samuelson, L. C., Yule, D. I., Ernst, S. A. and Williams, J. A. (1997). Overexpression of Rab3D enhances regulated amylase secretion from pancreatic acini of transgenic mice. *J. Clin. Invest.* **100**, 3044-3052.

Petrache, H. I., Gouliaev, N., Tristram-Nagle, S., Zhang, R. T., Suter, R. M. and Nagle, J. F. (1998a). Interbilayer interactions from high-resolution x-ray scattering. *Phys. Rev. E* **57**, 7014-7024.

Petrache, H. I., Tristram-Nagle, S. and Nagle, J. F. (1998b). Fluid phase structure of EPC and DMPC bilayers. *Chem. Phys. Lipids* **95**, 83-94.

Petrache, H. I., Dodd, S. W. and Brown, M. F. (2000). Area per lipid and acyl length distributions in fluid phosphatidylcholines determined by (2)H NMR spectroscopy. *Biophys. J.* **79**, 3172-3192.

Porter, F. D. (2000). RSH/Smith-Lemli-Opitz syndrome: a multiple congenital anomaly/mental retardation syndrome due to an inborn error of cholesterol biosynthesis. *Mol. Genet. Metab.* **71**, 163-174.

Rand, P., Fuller, N. L., Gruner, S. M. and Parsegian, V. A. (1990). Membrane curvature, lipid segregation. and structural transitions for phospholipid under dual-solvent stress. *Biochemistry* **29**, 76-87.

Rawicz, W., Olbrich, K. C., McIntosh, T., Needham, D. and Evans, E. (2000). Effect of chain length and unsaturation on elasticity of lipid bilayers. *Biophys. J.* **79**, 328-339.

Schneider, S. W., Sritharan, K. C., Geibel, J. P., Oberleithner, H. and Jena, B. P. (1997). Surface dynamics in living acinar cells imaged by atomic force microscopy: identification of plasma membrane structures involved in exocytosis. *Proc. Natl. Acad. Sci. USA* **94**, 316-321.

Schrader, M. (2004). Membrane targeting in secretion. *Subcell. Biochem.* **37**, 391-421.

Seddon, J. M. (1990). Structure of the inverted hexagonal (HII) phase, and non-lamellar phase transitions of lipids. *Biochim. Biophys. Acta* **1031**, 1-69.

Thiele, C. and Huttner, W. B. (1998). Protein and lipid sorting from the trans-Golgi network to secretory granules-recent developments. *Semin. Cell Dev. Biol.* **9**, 511-516.

Tint, G. S., Irons, M., Elias, E. R., Batta, A. K., Frieden, R., Chen, T. S. and Salen, G. (1994). Defective cholesterol biosynthesis associated with the Smith-Lemli-Opitz syndrome. *N. Engl. J. Med.* **330**, 107-113.

Tooze, S. A. (1998). Biogenesis of secretory granules in the trans-Golgi network of neuroendocrine and endocrine cells. *Biochim. Biophys. Acta* **1404**, 231-244.

van Meer, G. (1993). Transport and sorting of membrane lipids. *Curr. Opin. Cell Biol.* **5**, 661-673.

Wang, C. C., Ng, C. P., Lu, L., Atlashkin, V., Zhang, W., Seet, L. F. and Hong, W. (2004). A role of VAMP8/endobrevin in regulated exocytosis of pancreatic acinar cells. *Dev. Cell* **7**, 359-371.

Wang, Y., Thiele, C. and Huttner, W. B. (2000). Cholesterol is required for the formation of regulated and constitutive secretory vesicles from the trans-Golgi network. *Traffic* **1**, 952-962.

Wassif, C. A., Zhu, P., Kratz, L., Krakowiak, P. A., Battaile, K. P., Weight, F. F., Grinberg, A., Steiner, R. D., Nwokoro, N. A., Kelley, R. I. et al. (2001). Biochemical, phenotypic and neurophysiological characterization of a genetic mouse model of RSH/Smith-Lemli-Opitz syndrome. *Hum. Mol. Genet.* **10**, 555-564.

Wassif, C. A., Vied, D., Tsokos, M., Connor, W. E., Steiner, R. D. and Porter, F. D. (2002). Cholesterol storage defect in RSH/Smith-Lemli-Opitz syndrome fibroblasts. *Mol. Genet. Metab.* **75**, 325-334.

Witsch-Baumgartner, M., Ciara, E., Loffler, J., Menzel, H. J., Seedorf, U., Burn, J., Gillessen-Kaesbach, G., Hoffmann, G. F., Fitzky, B. U., Mundy, H. et al. (2001). Frequency gradients of DHCR7 mutations in patients with Smith-Lemli-Opitz syndrome in Europe: evidence for different origins of common mutations. *Eur. J. Hum. Genet.* **9**, 45-50.

Xu, X., Bittman, R., Duportail, G., Heissler, D., Vilcheze, C. and London, E. (2001). Effect of the structure of natural sterols and sphingolipids on the formation of ordered sphingolipid/sterol domains (rafts). Comparison of cholesterol to plant, fungal, and disease-associated sterols and comparison of sphingomyelin, cerebrosides, and ceramide. *J. Biol. Chem.* **276**, 33540-33546.

Zhang, C. F., Dhanvantari, S., Lou, H. and Loh, Y. P. (2003). Sorting of carboxypeptidase E to the regulated secretory pathway requires interaction of its transmembrane domain with lipid rafts. *Biochem. J.* **369**, 453-460.